Astronomy & Astrophysics manuscript no. VanLoo February 5, 2008
(DOI: will be inserted by hand later)

Non-thermal radio emission from single hot stars

S. Van Loo, M.C. Runacres, and R. Blomme

Royal Observatory of Belgium, Ringlaan 3, B-1180 Brussel, Belgium

Received / Accepted

Abstract. We present a theoretical model for the non-thermal radio emission from single hot stars, in terms of synchrotron radiation from electrons accelerated in wind-embedded shocks. The model is described by five independent parameters each with a straightforward physical interpretation. Applying the model to a high-quality observation of Cyg OB2 No. 9 (O5 If), we obtain meaningful constraints on most parameters. The most important result is that the outer boundary of the synchrotron emission region must lie between 500 and 2200 stellar radii. This means that shocks must persist up to that distance. We also find that relatively weak shocks (with a compression ratio < 3) are needed to produce the observed radio spectrum. These results are compatible with current hydrodynamical predictions. Most of our models also show a relativistic electron fraction that increases outwards. This points to an increasing efficiency of the acceleration mechanism, perhaps due to multiple acceleration, or an increase in the strength of the shocks. Implications of our results for non-thermal X-ray emission are discussed.

Key words. stars: early-type – stars: mass-loss – stars: winds, outflows – radio continuum: stars – radiation mechanisms: non-thermal

1. Introduction

Many hot stars of spectral type O and B are observable at radio wavelengths, due to thermal emission from the circumstellar ionized gas in the stellar wind. The thermal radiation is free-free emission (Bremsstrahlung) from an electron accelerated in the Coulomb field of an ion. The emergent radio spectrum has a characteristic spectral index[1] $\alpha \approx 0.6$ (Wright & Barlow 1975), which fits the observations for most O stars quite well.

However, 25% of the brightest O stars have a radio spectrum with a spectral index which is very different from the thermal wind emission (Abbott et al. 1984). It is believed that this *non-thermal* radio emission is synchrotron radiation by relativistic electrons (White 1985). The preferred mechanism to accelerate electrons to relativistic energies is particle acceleration in shocks (Fermi 1949), as shocks are known to exist in stellar winds. In single stars, shocks are generated by the instability of the driving mechanism of the wind (Owocki & Rybicki 1984). For binaries, shocks also arise in colliding winds (Eichler & Usov 1993). Non-thermal radio emission from colliding wind binaries has been further investigated by Dougherty et al. (2003). In this paper we limit ourselves to single stars.

Besides shocks, a magnetic field is needed to produce a synchrotron spectrum. Magnetic fields of normal hot stars are below current detection limits ($\sim$ 100 Gauss). It is plausible that a small magnetic field is present in the star, either the fossil magnetic field, or a field created by a dynamo mechanism (MacGregor & Cassinelli 2003).

The model proposed by White (1985) was further developed by Chen & White (1991, 1994), who showed that a synchrotron model can successfully reproduce the radio spectrum of 9 Sgr and Cyg OB2 No. 9.

In the present paper, we investigate what properties a synchrotron model should have in order to reproduce an observed non-thermal radio spectrum. More specifically, we look at *all* models that fit a given set of observations and thus derive the permitted range of a number of parameters. The stringency of the constraint on the parameters depends critically on the quality of the available observations, as well as on the number of observed wavelengths. We selected Cyg OB2 No. 9 as the object of this study because a set of three simultaneous observations (at 2, 6 and 20 cm) with small error bars is available.

For the sake of clarity it is desirable that the properties of the model be contained in a limited number of parameters with a clear physical interpretation. Rather than calculating the momentum distribution of relativistic electrons from a model of the shocks in the stellar wind, we use a power-law dependence on the compression ratio. The uncertainty about the exact shock structure is so large that an ab initio calculation of the momentum distribution would lead to a greater complexity of the model without increasing its physical accuracy.

The remainder of this paper is organised as follows. In Sect. 2 we describe the model for the synchrotron radiation in detail. The effect of cooling mechanisms on the momentum distribution is investigated in Sect. 3. In Sect. 4 we apply the

Send offprint requests to: S. Van Loo, e-mail: Sven.VanLoo@oma.be

[1] The radio spectral index α is defined by $F_\nu \propto \nu^\alpha \propto \lambda^{-\alpha}$

model to Cyg OB2 No. 9. Finally, we discuss the results in Sect. 5 and give some conclusions.

2. The model

2.1. Power

In the presence of shocks and a magnetic field, electrons are accelerated to high velocities (Bell 1978) through the first-order Fermi mechanism (Fermi 1949) and emit synchrotron radiation as they gyrate around the magnetic field lines at relativistic velocities. The synchrotron power radiated per unit volume per unit frequency by a single electron with momentum p, moving in a magnetic field B (dependent on distance r) with pitch angle θ, can be expressed as (Westfold 1959)

$$P_\nu(p,\theta,r) = \frac{\sqrt{3}e^3}{m_e c^2} B f(\nu,p)\sin\theta \times F\left(\frac{\nu}{f^3(\nu,p)\nu_s(p,r)\sin\theta}\right), \quad (1)$$

where m_e and e are the electron mass and charge, c the speed of light, ν the frequency, $F(x) = x\int_x^\infty d\eta K_{5/3}(\eta)$ and $K_{5/3}$ the modified Bessel function. For the meaning of $f(\nu,p)$, see Sect. 2.2. The synchrotron power spectrum extends up to frequencies of order ν_s before falling away, with the critical frequency ν_s defined as

$$\nu_s(p,r) = \frac{3}{4\pi}\frac{eB}{m_e c}\left(\frac{p}{m_e c}\right)^2. \quad (2)$$

2.2. Razin effect

The presence of $f(\nu,p)$ in the synchrotron power is a consequence of the Tsytovitch-Razin effect (or Razin effect for short; Tsytovitch 1951; Razin 1960). Relativistic beaming plays a dominant rôle in the explanation of synchrotron emission. In the presence of a cold plasma, the refraction index is smaller than unity. This increases the beaming angle, thereby reducing the beaming effect. Thus the synchrotron emitting power is greatly reduced. Ginzburg & Syrovatskii (1965) expressed $f(\nu,p)$ as

$$f(\nu,p) = \left[1 + \frac{\nu_0^2}{\nu^2}\left(\frac{p}{m_e c}\right)^2\right]^{-1/2}, \quad (3)$$

with $\nu_0 = \sqrt{\frac{n_e e^2}{\pi m_e}}$ the plasma frequency and n_e the number density of thermal electrons.

In the absence of the Razin effect ($f(\nu,p) = 1$), the essential part of the synchrotron emission of an individual electron with momentum p is emitted below the critical frequency ν_s, with a maximum at

$$\nu = 0.29\nu_s\sin\theta \approx 1.3\left(\frac{B\sin\theta}{1\ \text{Gauss}}\right)\left(\frac{p}{m_e c}\right)^2 \text{MHz}. \quad (4)$$

Away from the maximum, the synchrotron radiation falls off rapidly. We can therefore use Eq. (4) to estimate the momentum range relevant for the radio spectrum. For a magnetic field of 0.1 Gauss, radiation between 2 − 20 cm (15 − 1.4 GHz) comes from electrons with momenta between $\approx$ 50 − 150 MeV/c, where we set $\sin\theta = 1$.

From Eq. (3) we see that the Razin effect is important when $\nu \ll \nu_0 p/(m_e c)$. If on the other hand $\nu \gg \nu_0 p/(m_e c)$, the influence of the Razin effect is small. We can then use Eq. (2) to substitute p and find the frequencies for which the influence of the Razin effect is small. In the literature (e.g. Ginzburg & Syrovatskii 1965), this is given by

$$\nu \gg 20\frac{n_e}{B} \quad (5)$$

where, in view of the approximate nature, the factor 0.29 has not been taken into account. In a typical hot-star wind, the thermal electron density at 100 R_* is of order 10^7 cm^{-3}. For a magnetic field of 0.1 Gauss this means that the Razin effect begins to suppress radiation at wavelengths larger than 15 cm, well within the observable range. For smaller magnetic fields, the radiation is suppressed at even smaller wavelengths e.g. 1.5 cm for a 0.01 Gauss field.

2.3. Flux

The synchrotron emissivity of a distribution $N(p,r)$ of relativistic electrons can be expressed as

$$j_\nu(r) = \frac{1}{4\pi}\int_{p_0}^{p_c} \mathrm{d}p N(p,r)\bar{P_\nu}(p,r), \quad (6)$$

where $\bar{P_\nu}(p,r)$ is the synchrotron power $P_\nu(p,\theta,r)$ averaged over solid angle assuming that the electron velocity distribution is locally isotropic. The low (high) momentum cut-off of the electron distribution is defined by p_0 (respectively p_c). We will specify the cut-off values in Sect. 3.

The emergent flux is given by

$$F_\nu = \frac{1}{D^2}\int_{R_\nu}^{R_{\max}} \mathrm{d}r 4\pi r^2 j_\nu(r), \quad (7)$$

where D is the distance to the star. The integration boundaries reflect the fact that, at any given radio frequency, only a limited part of the wind contributes to the flux. The choice of these boundaries is rather subtle. The lower boundary mimics the effect of the large free-free optical depth of the wind, which effectively shields the inner part of the synchrotron emitting region from observation. The lower boundary must increase with increasing wavelength, to reflect the increasing free-free optical depth of the wind. It is customary (e.g. White 1985) to use the characteristic radius from Wright & Barlow (1975) as the lower boundary. However, this radius corresponds to a small optical depth ($\tau_\nu \approx 0.25$) and was introduced to produce the correct *thermal* radio flux with a simple one-dimensional integral. Its physical meaning is often misstated and is actually quite limited. It is *not* true that all observed radio emission originates from above R_ν. It is quite easy to replace Eq. (7) by the correct expression which is, however, rather cumbersome. We therefore relegate its derivation to Appendix A and prefer to use the simple approximation Eq. (7) in the discussion of our results. The calculations were done using the exact expression given in Eq. (A.6).

As for the outer integration boundary, it is well known that instability-generated shocks decay as they move out with the wind (e.g. Runacres & Owocki 2002). It can therefore be expected that they eventually become too weak to accelerate electrons to relativistic energies. Because relativistic electrons rapidly lose momentum as they move away from the shock (Sect. 3.4), the outer boundary of the synchrotron emission region ($R_{\max}$) can also be visualised as the position of the last shock strong enough to accelerate electrons to relativistic energies. It does not depend on frequency and is a fundamental parameter of our models.

The total emergent flux has a minor contribution from free-free emission by *thermal* electrons. This contribution is calculated using the Wright & Barlow formalism (Wright & Barlow 1975) and added to the non-thermal flux.

2.4. Number distribution and magnetic field

In order to derive an explicit expression for the emissivity, we need to specify the number distribution $N(p, r)$ and the magnetic field $B(r)$.

It was shown by Bell (1978) that the acceleration of electrons through the Fermi mechanism results in a power-law momentum distribution with exponent n, where n is a function of the compression ratio χ of the shock: $n = (\chi + 2)/(\chi - 1)$. For reasons of simplicity, we also assume that the distribution is a continuous function of distance, given by a power law with exponent δ. $N(p, r)$ is then expressed as

$$N(p, r) = N_0 \left(\frac{r}{R_*}\right)^{-\delta} p^{-n}, \tag{8}$$

where N_0 is a normalisation constant related to the number of relativistic electrons. The total number of relativistic electrons at the stellar surface is given by $\int_{p_0}^{p_c} \mathrm{d}p N_0\, p^{-n}$. This gives

$$N_0 = f_* n_{\mathrm{e}}^* (n-1)\, p_0^{n-1}, \tag{9}$$

where we introduced f_* and n_{e}^* as the fraction of relativistic electrons and the total electron number density at the stellar surface. We also assumed $p_c \gg p_0$ (see Sect. 3). The radial variation of the fraction of relativistic electrons in the wind is described by $f_*(r/R_*)^{-\delta+2}$. It must be emphasised that f_* is merely a parameter used to set the overall level of this fraction. It should not be too strictly interpreted as a physical quantity. Indeed, close to the stellar surface, the relativistic electron population may be strongly suppressed by inverse Compton cooling in the intense UV-radiation. Therefore f_* need not represent the actual relativistic electron fraction at the stellar surface.

For n_{e}^* we use

$$n_{\mathrm{e}}^* = \frac{\gamma \dot{M}}{4\pi R_*^2 v_\infty \mu m_{\mathrm{H}}}, \tag{10}$$

where $\dot{M}$ is the mass loss rate, v_∞ the terminal velocity of the stellar wind, m_{H} the mass of a hydrogen atom, γ the mean number of electrons per ion and μ the mean ionic weight. For simplicity we assume $\gamma = 1$ and $\mu = 1.4$. Note that n_{e}^* is not the actual electron density at the stellar surface (as the variation of the velocity has not been taken into account), but merely provides the correct scaling factor for the electron density at large distances.

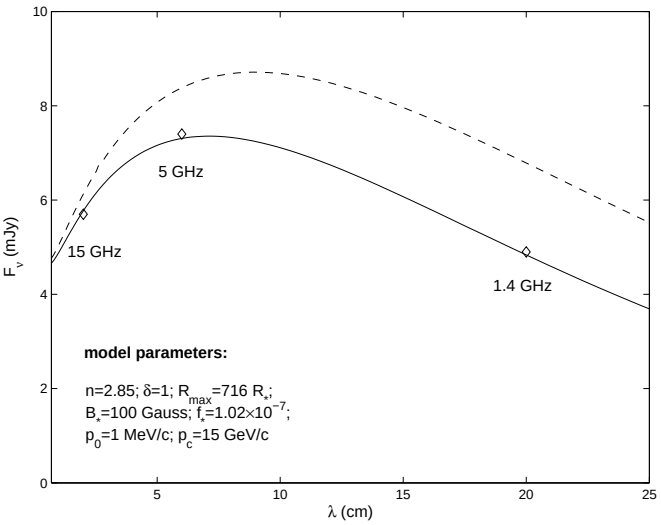

Fig. 1. The full line represents a model that fits the VLA-observations (21 Dec 1984) for Cyg OB2 No. 9 (Bieging et al. 1989), while the dashed line neglects the Razin effect. The diamonds are the observations and the error bar is given by the size of the symbol. The stellar parameters are listed in Table 1.

In Eq. (1) the magnetic field B must be specified. Unfortunately, the magnetic fields of hot stars are below current detection limits. Therefore, we can say little about their radial dependence. For want of anything better, we will adopt the expression (Weber & Davis 1967)

$$B(r) = B_* \frac{v_{\mathrm{rot}}}{v_\infty} \frac{R_*}{r}, \tag{11}$$

where B_* is the surface magnetic field and v_{rot} the rotational velocity of the star. This expression is only valid at large distances from the star ($r \geq 10\, R_*$), which covers the region where the synchrotron radiation is emitted. For the surface magnetic field, the detection limit, which is of order $\sim$ 100 Gauss (Mathys 1999), serves as an upper limit. A tentative lower limit can be derived from the synchrotron emission itself. At local magnetic fields smaller than $\sim$ 0.005 Gauss at 100 R_*, all radio emission would be suppressed by the Razin effect. Using Eq. (11) and $v_{\mathrm{rot}}/v_\infty = 250/2900$, this translates to a surface magnetic field of order 5 Gauss.

Once a choice for the parameters B_*, n, δ, $R_{\max}$, f_*, p_0 and p_c has been made, Eq. (A.6) can be integrated numerically. The total emergent flux (i.e. non-thermal + thermal) for one such model is shown in Fig. 1.

2.5. Tests

If we neglect the Razin effect and approximate the cut-off values p_0 and p_c by 0 and ∞, the emissivity can be calculated analytically (e.g. Rybicki & Lightman 1979) from Eq. (6). The expression for the emissivity then becomes a power law: $j_\nu \propto \nu^{-(n-1)/2}$. Introducing this into Eq. (7), an analytic expression is found for the synchrotron flux (Ginzburg & Ozernoy 1966),

which can then be compared to the results of the numerical code.

In the code, the momentum integral of the emissivity, given in Eq. (6), is computed using the trapezoidal rule and the step size is refined until it reaches a desired fractional precision of 10^{-3}. This emissivity has to be calculated at different positions in the wind. Then, the spatial integral of the flux, Eq. (7), is treated in the same way as the momentum integral, but up to a precision of order 1%. The number distribution is given by Eq. (8), while the mean synchrotron power $\bar{P}_\nu$ is calculated using a linear interpolation between tabulated values. This way, the mean synchrotron power $\bar{P}_\nu$ needs to be calculated only once (as a function $\nu/f^3(\nu,p)\nu_s(p,r)$) which reduces the calculation time significantly. The next step is to approximate the momentum cut-off values, p_0 and p_c by 0 and ∞. We start with $p_0 = 1$ MeV/c and $p_c = 10$ GeV/c and then we expand the interval by doubling the value for p_c and halving the value of p_0 until the solution for the integral has converged. We can then compare the numerical results to the analytic solution. We calculated 5000 models with B_* in the range 10–100 Gauss, n between 1.5–7.5, δ between 0–5 and $R_{\max}$ between 100–10 000 R_*. The relative errors of the numerical models compared to the analytic models did not exceed the 1% level.

3. Cooling mechanisms

3.1. Practical momentum limits

In this section we determine practical integration limits for the momentum distribution, which we need to calculate the synchrotron emissivity, given by Eq. (6).

Relativistic electrons can lose their energy through a variety of cooling mechanisms. Coulomb collisions, inverse Compton scattering, adiabatic cooling, synchrotron cooling and Bremsstrahlung cooling can all play a rôle. The effect of these cooling mechanisms has been discussed in detail by Chen (1992). At the high energy end of the spectrum, electrons are mainly cooled by inverse Compton scattering. This sets an upper limit p_c to the momentum range. At the low (non-relativistic) end of the spectrum, Coulomb collisions are the dominant cooling mechanism. This sets a lower boundary p_0 to the momentum range. As momenta below p_0 or above p_c cannot occur, the momentum range is limited to $[p_0, p_c]$. Only a fraction of this range actually contributes to observable radio emission, as can be seen from Eq. (4). For $B_* = 100$ Gauss and assuming that the synchrotron radiation is formed somewhere between 30 and 1000 R_* (see Sect. 4.2.1), the range of momenta that contribute to the observable radio flux is 30 – 500 MeV/c. It is therefore convenient to introduce an ad-hoc integration interval $[p_1, p_2]$ that is contained in $[p_0, p_c]$ but is large enough to include all momenta that produce observable radio emission. Within these constraints we choose $[p_1, p_2]$ as small as possible, for reasons of computational efficiency. The exact choice of p_1 and p_2 is unimportant. In the following section we shall derive values of p_1 and p_2 that can be used in the models.

3.2. Low momentum cut-off

Synchrotron emission at wavelengths shorter than 20 cm is produced by relativistic electrons with momenta above $\approx$ 30 MeV/c. Any value $p_1 \ll 30$ MeV/c can therefore be used as a practical lower limit to the momentum range. A convenient choice of p_1 is $p_1 = 1$ MeV/c. Although the choice of p_1 does not influence the flux, it does influence the number of electrons (as seen in Eq. (9)).

We still need to check whether electrons of momentum p_1 exist, i.e. whether $p_1 > p_0$ (where p_0 is the momentum cut-off set by Coulomb cooling). We therefore compare the acceleration time of electrons with momentum $p_1 = 1$ MeV/c with the time-scale for Coulomb collisions of electrons with thermal ions. Collisions happen on time-scales given by (Spitzer 1956)

$$t_{\rm D} = \frac{m_{\rm e}^2 v^3}{8\pi e^4 n_{\rm g} \ln\Lambda}, \tag{12}$$

where v is the speed of the relativistic electrons, $n_{\rm g}$ the number density of the ions and $\ln\Lambda$ the Coulomb logarithm. In hot-star winds the Coulomb logarithm is ~ 10. The time to accelerate an electron up to a momentum p is given by (Chen 1992)

$$t_{\rm acc} = \frac{3}{2\Delta u(r)}\frac{pc}{eB}, \tag{13}$$

where $\Delta u(r)$ is the shock velocity difference at radius r. For an electron of 1 MeV/c at a radial distance of 100 R_* where the number density of the ions is $n_{\rm g} = 10^7$ cm^{-3} and $B = 0.1$ Gauss, we find $t_{\rm D} \approx 10^5$ s, while $t_{\rm acc} \approx 5 \times 10^{-3}$ s (where we assume $\Delta u = 100$ km s^{-1}). Further out in the wind the ratio $t_{\rm D}/t_{\rm acc}$ increases. This means that electrons with momentum 1 MeV/c will not be Coulomb-cooled significantly.

3.3. High momentum cut-off

Synchrotron emission at wavelengths greater than 2 cm is produced by relativistic electrons with momenta below $\approx$ 500 MeV/c (for $B_* = 100$ Gauss). Any value $p_2 \gg 500$ MeV/c can therefore be used as a practical upper limit to the momentum range, providing $p_2 < p_c$ (where p_c is the high momentum cut-off).

The highest momentum attainable for relativistic electrons is determined by the balance between acceleration and inverse Compton scattering at the shock. This results in a maximum attainable momentum p_c, that can be expressed as (Chen 1992)

$$p_c(r) = m_e c \left(4\pi \frac{eB(r)}{\sigma_{\rm T} L_*}\Delta u(r) r^2\right)^{1/2}, \tag{14}$$

where $\sigma_{\rm T}$ is the Thomson cross section and L_* the stellar bolometric luminosity. Using typical hot star values ($L_* = 10^6$ L$_\odot$, $v_\infty = 2\,500$ km s^{-1}, $v_{\rm rot} = 200$ km s^{-1}, $R_* = 20$ R$_\odot$ and $\Delta u(r) = 100$ km s^{-1}), we can estimate a numerical value for the high momentum cut-off,

$$p_c(r) \approx 0.97 \frac{\rm GeV}{c}\left(B_* \frac{r}{R_*}\right)^{1/2}. \tag{15}$$

For $B_* = 100$ Gauss and $r = 10\ R_*$, Eq. (15) gives $p_c = 30$ GeV/c. At larger distances from the star p_c is larger. A practical choice for p_2 that satisfies $p_2 < p_c$ is $p_2 = 15$ GeV/c.

Table 1. Relevant stellar parameters for Cyg OB2 No. 9 adopted in this paper. The numbers are taken from Bieging et al. (1989, BAC), Leitherer (1988, L) and Herrero et al. (1999, HCVM).

Parameter		Ref.
$v_{\rm rot} \sin i$ (km s^{-1})[a]	145	BAC
$T_{\rm eff}$ (K)[b]	44 500	HCVM
R_* ($R_\odot$)	22	HCVM
d (kpc)	1.82	BAC
v_∞ (km s^{-1})	2 900	L
$\dot{M}$ ($M_\odot$ yr^{-1})	2.0×10^{-5}	L

[a] We follow White (1985) in assuming that $v_{\rm rot} = 250$ km s^{-1}, which is not in contradiction with the value for $v_{\rm rot} \sin i$.
[b] The wind temperature is assumed to be 0.3 times the stellar effective temperature (Drew 1989).

Table 2. With the stellar parameters for Cyg OB2 No. 9 given in Table 1, we have the following values for the characteristic radius R_ν (see Eq. (A.7)) and for the free-free emission from the wind (Wright & Barlow 1975). For simplicity we assume $\gamma = 1, Z^2 = 1$ and $\mu = 1.4$. As a reference we also give the values of the non-thermal component to the flux and the observed flux with error bars.

λ (cm)	ν (GHz)	$R_\nu(T_{\rm wind})$ (R_*)	$F_\nu^{\rm ff}$ (mJy)	$F_\nu^{\rm nt}$ (mJy)	$F_\nu^{\rm obs}$ (mJy)
2	15	124	1.1	4.6	5.7 ±0.1
6	5	266	0.6	6.8	7.4 ±0.1
20	1.4	614	0.3	4.6	4.9 ±0.1

Now that a choice has been made for p_1 and p_2, the independent parameters are reduced to B_*, n, δ, $R_{\rm max}$ and f_*.

3.4. Emitting region

We have estimated practical upper and lower limits to the momentum range that are compatible with the high and low momentum cut-offs due to Compton and Coulomb cooling, respectively. Of course, cooling can also change the distribution between these limits. Specifically, as the relativistic electrons move away from the shock in which they were accelerated, inverse Compton scattering will rapidly cool the most energetic electrons. Inverse Compton scattering does not change the total number of relativistic particles, but quickly reduces their energy below the energy of observable radio emission. Thus, the synchrotron emitting gas is concentrated in more or less narrow regions behind the shocks. For the sake of simplicity we neglect this layered structure of the synchrotron emitting region and assume a continuous volume of relativistic particles. The adequacy of this assumption is discussed in Sect. 5.

4. Application and results

4.1. Cyg OB2 No. 9: 21 Dec 1984 data

We can now apply the model to Cyg OB2 No. 9 (O5 If). It was first discovered by Abbott et al. (1984) that the spectral index of its radio emission does not follow the $\alpha = 0.6$ law expected for a thermal wind source (see Fig. 1). Also, the radio emission of Cyg OB2 No. 9 is highly variable. On one occasion the radio spectrum even showed a typical free-free spectrum (with $\alpha = 0.6$). If we determine the mass loss rate from this radio observation, we find the same value as derived from Hα (Leitherer 1988). So we can assume that at that time we saw the underlying free-free emission from the stellar wind. Of the observational radio data that are available for Cyg OB2 No. 9, we will use the observation that has detections of emission in three radio wavelength bands. We chose the 21 Dec 1984 observation with the VLA (Bieging et al. 1989) because of its small error bars on the detections. By fitting these observations we can derive the solution space of the model parameters. The stellar parameters adopted in our model are listed in Table 1.

4.2. Results

We recall that the parameter space is spanned by n, δ, f_*, $R_{\rm max}$ and B_*. The parameters have a straightforward interpretation: n corresponds to a typical compression ratio in the synchrotron formation region, δ describes the spatial dependence of the number distribution, f_* describes the fraction of relativistic electrons at the surface and $R_{\rm max}$ is the outer boundary of the synchrotron emission region. We take $B_* = 100$ Gauss in the fitting procedure, which corresponds to a local magnetic field of $B = 1.7 \times 10^{-2}$ Gauss at $r = 500\ R_*$.

We calculate the synchrotron flux in the three wavelengths for a grid in n, δ, $R_{\rm max}$ and f_* and select those combinations of the parameters that fit the VLA-observations within the error bars. This procedure produces a strong constraint on n, δ and $R_{\rm max}$, but not on f_*. The parameter f_* is well constrained locally (i.e. for each combination of n, δ and $R_{\rm max}$), but not globally (i.e. for the entire range of n, δ and $R_{\rm max}$). This parameter does play a minor rôle in limiting the other parameters as the number of relativistic electrons cannot exceed the total number of electrons. In principle this limitation depends on p_1, but in practice the effect is minimal. All possible combinations of n, δ and $R_{\rm max}$ lie within the boomerang-shaped region in Fig. 2.

4.2.1. $R_{\rm max}$

The most important result from Fig. 2 is that $R_{\rm max}$ *is well constrained* and almost not influenced by n and δ. The outer boundary of the synchrotron emitting region must lie between 520 R_* and 750 R_*. To understand this result, it is important to realise that the different wavelengths play a different rôle in the fitting procedure. The fluxes at 2 and 6 cm constrain n, δ and f_*. The parameters n and δ determine the slope between 2 and 6 cm and f_* sets the global flux level. Note that different combinations of n and δ can give the same slope. The effect of $R_{\rm max}$ on the slope is negligible. The flux at 20 cm is fitted by the only remaining parameter $R_{\rm max}$. The strong dependence of the 20 cm-flux on $R_{\rm max}$ is due to the larger free-free opacity at larger wavelengths. This means that more of the synchrotron emitting region is shielded at 20 cm than at 2 and 6 cm. This also explains why $R_{\rm max}$ has only a small influence on the 2 and 6 cm-fluxes. Note that the range in $R_{\rm max}$ (520 – 750 R_*) extends below the

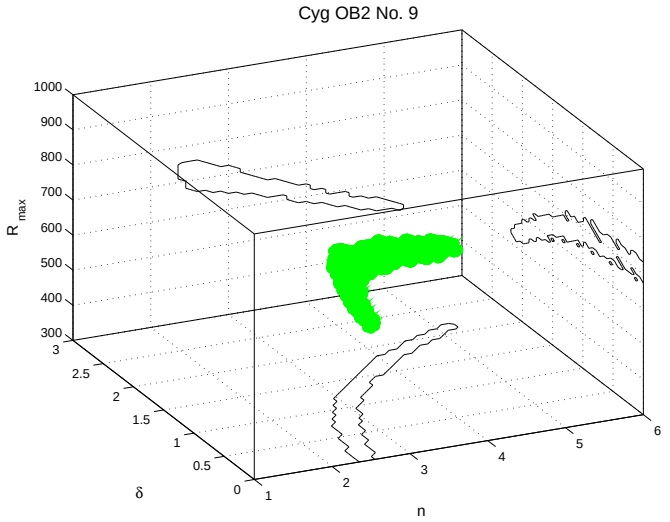

Fig. 2. All the combinations of n, δ and $R_{\max}$ with $B_* = 100$ Gauss that fit the VLA-observations (21 Dec 1984) for Cyg OB2 No. 9 lie within the boomerang-shaped region. Projections on different planes are plotted to situate the solutions in the parameter space.

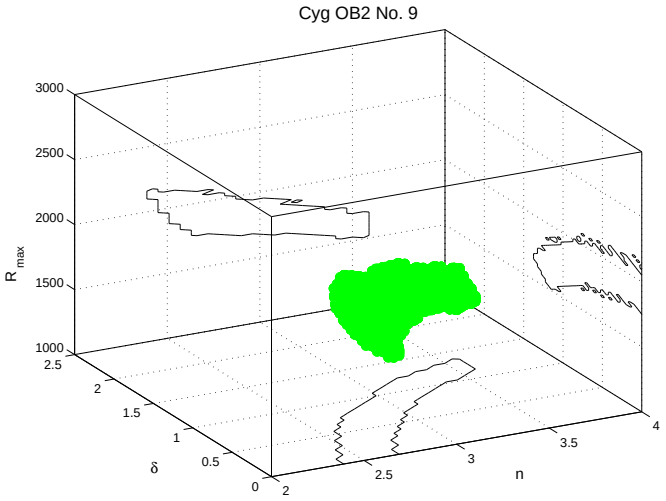

Fig. 3. Similar figure as Fig. 2, but now calculated for a surface magnetic field $B_* = 10$ Gauss (Note the different scales compared to Fig. 2).

characteristic radio radius at 20 cm ($R_\nu(20\text{ cm}) = 614\,R_*$). This is not a contradiction as radio emission from below R_ν can be detected (see Sect. 2.3).

While $R_{\max}$ is insensitive to n and δ, it depends strongly on the magnetic field. Assuming a smaller surface magnetic field of 10 Gauss rather than the 100 Gauss used previously, we find a larger value of $R_{\max}$ (see Fig. 3). $R_{\max}$ is still well constrained, but now the range extends from 1 500 R_* up to 2 200 R_*. The larger value of $R_{\max}$ is caused by the greater importance of the Razin effect at lower magnetic fields. The 20 cm-flux is already greatly reduced by the Razin effect. To replenish the photons taken away by the Razin effect, the synchrotron emitting region must be larger than the value of $R_{\max}$ found for a magnetic field of 100 Gauss. It is not possible to fit the observations with a surface magnetic field of 5 Gauss, because essentially all radio emission is suppressed by the Razin effect (Sect. 2.4). In this sense the value of $B_* = 10$ Gauss can be considered a lower limit for the surface magnetic field, and likewise the value found for $R_{\max}$ is an upper limit to the outer boundary of the synchrotron emission region.

4.2.2. n and δ

Fig. 2 shows solutions with n extending from 2.5 to 5. Using the relation $\chi = (n + 2)/(n - 1)$, this translates to compression ratios from $\chi = 3$ (moderately strong shocks) to $\chi = 1.75$ (weak shocks). Note that strong shocks ($\chi = 4$) cannot explain the observations. This is consistent with what was found by Rauw et al. (2002), who applied a similar model to 9 Sgr. Since time-dependent hydrodynamical simulations (e.g. Runacres & Owocki 2002) show a variety of shocks (and compression ratios) in the stellar wind, χ is some kind of compression ratio average. Stronger shocks however produce more radio emission than weaker shocks, because they accelerate more of the electrons into the momentum range where synchrotron radiation is emitted at radio wavelengths. Thus the synchrotron spectrum is dominated by the stronger shocks. Thus the value of χ we obtain should be interpreted as a maximum compression ratio in the wind, rather than a mean compression ratio.

Note that most solutions have δ-values lower than 2. This means that the fraction of relativistic electrons increases further in the wind. This is surprising as one would expect a constant efficiency of the acceleration mechanism or even a decreasing efficiency (due to the decay of the shocks in the wind). The increasing relativistic fraction points to an increasing acceleration efficiency. A possible explanation is multiple acceleration of the electrons by subsequent shocks. Thermal electrons are injected in the shock front and accelerated, but electrons, already accelerated by a previous shock, are also re-accelerated. This would increase the number of relativistic electrons toward the outer region of the stellar wind.

Another possible explanation is that, as hydrodynamical simulations show a variety of shocks, some stronger shocks might exist in the outer parts of the wind. This would increase the synchrotron emission which would show up as a $\delta < 2$ in the parametrisation of the current model.

4.2.3. Comparison with the Chen & White model

We can compare our results with the results found in Chen & White (1991, 1994). We looked at all the models that fit the observations of Cyg OB2 No. 9 and derived the permitted range of the model parameters. We used a power law to describe the number distribution of relativistic electrons. Chen & White calculated the number distribution from a model of shocks in the stellar wind. The parameters of their synchrotron model which reproduce the radio spectrum of Cyg OB2 No. 9 were $n = 2.6$, $\delta < 2$ and $R_{\max} = 500 R_*$. Even though we used different methods to describe the momentum distribution of relativistic electrons in the wind, the parameters of their synchrotron model are very similar and can be found near the solution space of our model.

5. Discussion and conclusions

In this paper we have presented a theoretical model for non-thermal radio emission from single hot stars, in terms of synchrotron emission from electrons accelerated in wind-embedded shocks. Applied to a specific observation of Cyg OB2 No. 9, the model produces constraints on almost all of its parameters (f_* being the only exception). A major result is that the outer boundary of the synchrotron emitting region ($R_{\rm max}$) is well constrained (520 – 750 R_* for B_* = 100 Gauss). As the efficiency of Compton cooling prevents relativistic electrons from carrying their kinetic energy far from the shock, this means that our models predict that shocks persist to at least 500 R_*. This is consistent with recent hydrodynamical calculations (Runacres & Owocki 2003).

Another interesting result is the absence of very strong shocks (those with compression ratio χ near 4) in the outer wind. We find shocks with $\chi = 3$ at most. This is consistent with the hydrodynamical prediction that shocks become weaker as they move out with the stellar wind.

Within the range of solutions we find both $\delta \approx 2$ and $\delta < 2$. The physical picture associated with these different values of δ is rather different too. The $\delta \approx 2$ solutions point to a constant fraction of relativistic electrons. It can be seen from Fig. 2 that they also correspond to weak shocks ($\chi \lesssim 2$). This offers a natural explanation for $R_{\rm max}$: the shocks weaken as they move out with the flow and beyond $R_{\rm max}$ they are to weak to produce significant synchrotron emission.

However, most of the solutions have $\delta < 2$, which points to the relativistic electron fraction increasing outwards. This could indicate an increasing compression ratio of the shocks, or at least the presence of a stronger shock in the outer part of the synchrotron emitting region. While this could incidentally have been the case at the time of observation, it does not sit well with the hydrodynamical prediction that shocks decay as they move outward. It is also hard to imagine why these shocks would rather suddenly disappear when they reach $R_{\rm max}$. A more plausible explanation of $\delta < 2$ is multiple acceleration: particles in the outer wind have had greater opportunity to pass through multiple shocks than particles in the inner wind. The $\delta < 2$ solutions are also those with larger compression ratios. In the case of multiple acceleration the momentum distribution is no longer a pure power law $\sim p^{-n}$, but a flatter function (White 1985). Simply put, this means that the momentum distribution for multiple acceleration by a number of weaker shocks resembles a distribution corresponding to a single stronger shock. This is then again consistent with the idea of an outer boundary of the synchrotron emitting region, as all the shocks involved in the acceleration are weak.

In this paper we have assumed a power-law momentum distribution with a single compression ratio, where all of the volume can contribute to the emission. The efficiency of inverse-Compton cooling, however, will limit the synchrotron emission region to more or less narrow layers behind the shocks. The primary effect of this is to reduce the number of electrons in the momentum range relevant for radio emission. This means that the values of f_* we find in our fitting procedure are underestimated as it is this parameter that sets the overall level of synchrotron emission, and must mimic the quenching of electrons by inverse Compton scattering. Because f_* is not well constrained by the adopted fitting procedure, this is of no consequence for our results. As a secondary effect, inverse-Compton cooling can also change the momentum distribution, as it affects the high momentum electrons more than the low momentum electrons. The importance of this effect will be investigated in a subsequent paper.

Hydrodynamical models predict a variety of compression ratios. Due to the strong dependence of the emission on the compression ratio, the strongest shock will dominate. In that case, the radiation would not come from the whole volume, but only from behind the strongest shocks. This may also explain the variability that is a characteristic feature of non-thermal radio emission (Bieging et al. 1989). As the stronger shocks move in and out of the synchrotron emitting region they lead to variability.

The presence of relativistic electrons in the wind will also lead to non-thermal X-rays, due to the inverse Compton process (Chen & White 1991). The non-thermal X-rays should show up as a hard X-ray tail in a spectrum. Clear evidence for such a non-thermal tail has remained elusive. Rauw et al. (2002) show that the hard X-ray tail of the non-thermal radio emitter 9 Sgr does not have the expected power-law dependence for non-thermal X-ray emission. The tail can also be modelled with a high-temperature ($\geq 2{\times}10^7$ K) *thermal* plasma. It should be noted that the non-thermal X-ray emission is formed much closer to the stellar surface (where there is an abundant supply of UV photons) than the non-thermal radio emission. One could therefore surmise that the shocks closer to the star are weaker and therefore result in an insufficient number of relativistic electrons to create detectable non-thermal X-rays. This suggestion, however, does not appear to be consistent with current hydrodynamical models, as the shocks are strongest in the inner wind and decay as they move outward. The hard X-ray tail of 9 Sgr could also be explained by colliding wind emission from a long-period binary companion (Rauw et al. 2002).

To obtain non-thermal radio emission, all that is required is a magnetic field and shocks in the wind. As both should be present in any early-type star, the question arises why not all these stars are non-thermal emitters. One possible answer is that the magnetic field in thermal stars is lower. A lower magnetic field means that less synchrotron radiation is generated and that the Razin effect is more efficient at suppressing it. This explanation suggests that searches to detect magnetic fields in O-type stars might have a better chance in non-thermal radio emitters. Another possible explanation is that the synchrotron emitting region (essentially determined by the characteristic free-free radius and $R_{\rm max}$) is too small, so that the synchrotron radiation emitted falls below detection levels.

Finally, one needs to ask the uncomfortable question whether there is any such thing as synchrotron emission from *single* O stars. For Wolf-Rayet stars, the connection between non-thermal emission and binarity is firmly established (Dougherty & Williams 2000). For O stars, the situation is less clear. Roughly half of the non-thermal O stars are not known to be members of a binary system. However, the truism that absence of evidence is not evidence of absence obviously holds.

Also, there is an indication that one of the archetypal single non-thermal O star, 9 Sgr, might actually be in a binary (Rauw et al. 2002). The possibility that all non-thermal emitting O stars are binaries cannot be excluded.

Acknowledgements. We thank S. Dougherty and J. Pittard for careful reading of the manuscript and S. Owocki for interesting discussions. SVL gratefully acknowledges a doctoral research grant by the Belgian State, Federal Office for Scientific, Technical and Cultural Affairs (OSTC). Part of this research was carried out in the framework of the project IUAP P5/36 financed by the OSTC.

Appendix A: Flux: exact and approximated integral

We calculate the flux following Wright & Barlow (1975) for the free-free emission, but we replace χB_ν, where χ is the free-free absorption coefficient and B_ν the source function (e.g. the Planck function), by the synchrotron emissivity j_ν. The exact integral for the flux is

$$F_\nu = \frac{1}{D^2}\int_0^{R_{\max}} \mathrm{d}q 2\pi q \int_{-\infty}^{\infty} \mathrm{d}l\, j_\nu[r(l)]\mathrm{e}^{-\tau_\nu(q,l)}, \tag{A.1}$$

where D is the distance to the star, q the impact parameter, l the distance along the line of sight with an observer at $l = -\infty$ and $R_{\max}$ the outer boundary for the synchrotron emission region. The optical depth $\tau_\nu(q,l)$ is defined as

$$\tau_\nu(q,l) = \int_{-\infty}^{l} \mathrm{d}l' \frac{K_{\mathrm{ff}}\gamma A^2}{(q^2+l'^2)^2}, \tag{A.2}$$

with $A = \dot{M}/(4\pi\mu m_H v_\infty)$, where the symbols have their usual meaning, and K_{ff} the free-free absorption coefficient given by Allen (1973). Note that by using 0 as the lower integral boundary in Eq. (A.1), we in fact replaced the star by stellar wind material. This mathematical simplification has no consequence as the free-free optical depth is so large that any contribution of the star can be neglected anyway.

The equation for $\tau_\nu(q,l)$ can be integrated to (using Abramowitz & Stegun 1965, 3.3.24)

$$\tau_\nu(q,l) = \frac{K_{\mathrm{ff}}\gamma A^2}{2q^3}\left[\frac{l/q}{1+\frac{l^2}{q^2}} + \arctan\left(\frac{l}{q}\right) + \frac{\pi}{2}\right]. \tag{A.3}$$

Introducing polar coordinates,

$$\begin{aligned} q &= r\sin\theta \\ l &= r\cos\theta \\ \mathrm{d}q\mathrm{d}l &= r\mathrm{d}r\mathrm{d}\theta \end{aligned} \tag{A.4}$$

we find

$$\tau_\nu(q,l) = \frac{K_{\mathrm{ff}}\gamma A^2}{2r^3\sin^3\theta}(\sin\theta\cos\theta - \theta + \pi) \tag{A.5}$$

and for the flux

$$F_\nu = \frac{1}{D^2}\int_0^{R_{\max}} \mathrm{d}r 4\pi r^2 j_\nu(r) G\left(\frac{r}{R_\nu}\right), \tag{A.6}$$

with R_ν the characteristic radius of emission (Wright & Barlow 1975) expressed as

$$R_\nu = \frac{4}{\Gamma\left(\frac{1}{3}\right)\left(\frac{\pi}{2}\right)^{2/3}}(K_{\mathrm{ff}}\gamma A^2)^{1/3}, \tag{A.7}$$

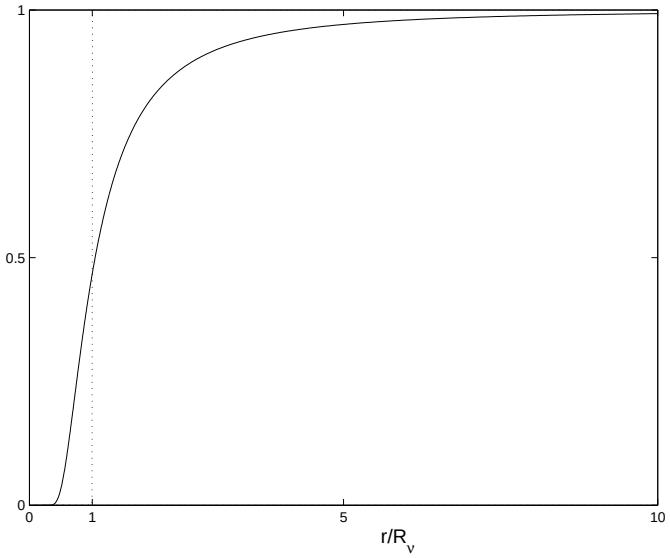

Fig. A.1. The full line is the geometric function $G(r/R_\nu)$, while the dashed line represents the Heaviside function.

and

$$G(x) = \frac{1}{2}\int_0^{\pi} \mathrm{d}\theta \sin\theta \times \exp\left[-\frac{\left(\Gamma\left(\frac{1}{3}\right)/8\right)^3\pi^2}{x^3\sin^3\theta}(\sin\theta\cos\theta - \theta + \pi)\right]. \tag{A.8}$$

The θ integration is only from 0 to π, because the original integral only considered positive q values (a factor of 2 was included in the original integration to compensate for this). The function $G(r/R_\nu)$ is plotted on Fig. A.1. Note that $G(r/R_\nu)$ can be approximated by a Heaviside function: $H = 0$ if $r < R_\nu$ and $H = 1$ if $r > R_\nu$. This brings us back to the approximation Eq. (7) for the flux. The function $G(r/R_\nu)$ needs to be calculated only once, so that evaluating Eq. (A.6) does not take significantly more time than Eq. (7).

References

Abbott, D. C., Bieging, J. H., & Churchwell, E. B. 1984, ApJ, 280, 671
Abramowitz, M., & Stegun, I. A. 1965, *Handbook of Mathematical Functions*, Dover Publications
Allen, C. W. 1973, *Astrophysical quantities*, The Athlone Press
Bell, A. R. 1978, MNRAS, 182, 147
Bieging, J. H., Abbott, D. C., & Churchwell, E. B. 1989, ApJ, 340, 518
Chen, W., & White, R. L. 1991, ApJ, 366, 512
Chen, W. 1992, Ph.D. Thesis John Hopkins Univ., Baltimore, MD., *Nonthermal radio, X-ray and gamma-ray emissions from chaotic winds of early-type, massive stars*
Chen, W., & White, R. L. 1994, Ap&SS, 221, 259
Dougherty, S. M., Pittard, J. M., Kasian, L., et al. 2003, A&A, 409, 217
Dougherty, S. M., & Williams, P. M. 2000, MNRAS, 319, 1005
Drew, J. E. 1989, ApJS, 71, 267
Eichler, D., & Usov, V. 1993, ApJ, 402, 271
Fermi, E. 1949, Phys. Rev., 74, 1169

Ginzburg, V. L., & Ozernoy, L. M. 1966, ApJ, 144, 599
Ginzburg, V. L., & Syrovatskii, S. I. 1965, ARA&A, 3, 297
Herrero, A., Corral, L. J., Villamariz, M. R., & Martin, E. L. 1999, A&A, 348, 542
Leitherer, C. 1988, ApJ, 326, 356
MacGregor, K. B., & Cassinelli, J. P. 2003, ApJ, 586, 480
Mathys, G. 1999, in Proc. IAU Coll. 169, Variable and Non-spherical Stellar Winds in Luminous Hot Stars, ed. B. Wolf, O. Stahl, & A. W. Fullerton, Lect. Notes Phys., 523, 95
Owocki, S. P., & Rybicki, G. B. 1984, ApJ, 284, 337
Rauw, G., Blomme, R., Waldron, W. L., et al. 2002, A&A, 395, 993
Razin, V.A. 1960, Radiophysica, 3, 584
Runacres, M. C., & Owocki, S. P. 2002, A&A, 381, 1015
Runacres, M. C., & Owocki, S. P. 2003, in preparation
Rybicki, G. B., & Lightman, A. P. 1979, *Radiative Processes in Astrophysics*, John Wiley & Sons
Spitzer, L. Jr. 1956, *Physics of Fully Ionized Gases*, Interscience Publishers, Inc.
Tsytovitch, V. N. 1951, Vestn.Mosk.Univ., 11, 27
Weber, E. J., & Davis, L. Jr. 1967, ApJ, 148, 217
Westfold, K. C. 1959, ApJ, 130, 241
White, R. L. 1985, ApJ, 289, 698
Wright, A. E., & Barlow, M. J. 1975, MNRAS, 170, 41